




Suppressing capacity fading and voltage decay of Ni-rich cathode material by dual-ion doping for lithium-ion batteries

Hao Liu¹, Ruikai Yang¹, Wen Yang¹, Changjiang Bai¹, Yong-Chun Li², Gongke Wang³, Yuxia Liu⁴, Wei Xiang⁵, Zhenguo Wu¹, and Xiaodong Guo^{1,*} 

¹ College of Chemical Engineering, Sichuan University, Chengdu 610065, People's Republic of China

² Institute of Chemistry, Humboldt University of Berlin, Brook-Taylor-Str. 2, 12489 Berlin, Germany

³ School of Materials Science and Engineering, Henan Normal University, Henan, China

⁴ The Key Laboratory of Life-Organic Analysis, Key Laboratory of Pharmaceutical Intermediates and Analysis of Natural Medicine, School of Chemistry and Chemical Engineering, Qufu Normal University, Qufu 273165, Shandong, China

⁵ College of Materials and Chemistry & Chemical Engineering, Chengdu University of Technology, Chengdu 610059, People's Republic of China

Received: 10 June 2020

Accepted: 31 August 2020

Published online:
20 October 2020

© Springer Science+Business Media, LLC, part of Springer Nature 2020

ABSTRACT

The Ni-rich cathodes are considered as the next generation candidate cathode material of lithium-ion batteries due to the high-energy-density and environmentally friendly. Unfortunately, the cathodes are up against severe structure instability at the repeated charge/discharge process, resulting in the attenuation of voltage and capacity. Herein, we proposed a novel strategy with uniform Al and Ti cations co-doping of $\text{LiNi}_{0.8}\text{Co}_{0.1}\text{Mn}_{0.1}\text{O}_2$ cathode. The modification strategy not only stabilizes the vulnerable layered structure but also mitigate voltage/capacity attenuation at different cutoff voltages. As a result, the modified cathode with trace content of Al and Ti cations co-doping can broaden the lithium ions diffusion channels, mitigate the structural collapse, and unfavorable phase transformation to some extent. Specifically, the modified sample exhibits remarkable enhanced electrochemical performance in discharge capacity and voltage retention of 76.75%, 98.78% at 1 C after 200 cycles. Even though at elevated voltage, the modified sample shows improved cycle life with a capacity retention of 70.93% after 200 cycles.

Handling Editor: Mark Bissett.

Address correspondence to E-mail: xiaodong2009@163.com

<https://doi.org/10.1007/s10853-020-05246-6>

Introduction

Nowadays, the lack of energy resources and environmental pollution has forced researchers to explore the next-generation cathode materials to replace the traditional commercial LiCoO₂ cathode. Ni-rich layered cathode with a high specific capacity, low cost, and environmentally friendly is one of the most promising cathodes [1–6], whereas the lack of stable structure and excellent cycle life cathode materials has also hindered its commercialization of LIBs. To pursuit of high capacity with more nickel content of cathode, the unsatisfied cycle life and poor thermal stability appear, especially at elevated high cutoff potential [7–9]. During the high-temperature calcination process, the nickel (II) in the transition metal sites easily migrates to lithium sites on account of a similar radius of Li and Ni (0.76 Å vs. 0.69 Å) which induce severe cations mixing region on the surface with inactive NiO-like phase [10–13]. Besides, the detrimental phase transformation of the spinel phase blocks the channels of lithium ions diffusion and induces the degradation of electrochemical performance. Moreover, the oxygen release aggravates the side reaction of cathode material and electrolyte at the in-depth delithiation process, even the fatal thermal runaway of LIBs [14, 15].

To address above the tough problems, numerous strategies have been proposed, which devote to decrease cation mixing or modify surface chemistry properties. Such as lattice element doping (Ti⁴⁺ [16], Al³⁺ [17], La³⁺ [18], Mg²⁺ [19], Zn²⁺ [20], Zr⁴⁺ [21], PO₄³⁻ [22]), surface coating (TiO₂ [23], ZrO₂ [24], CoF₂ [25], SnO₂ [26]), and so on. Although surface coating can suppress surface side reactions by constructing an inactive coating layer at the beginning of the cycle, severe cation mixing resulting from TM ions migration in bulk at extending cycles limits any improvement [27]. Therefore, to fundamentally address these problems of layered Ni-rich cathodes, it is necessary to consider the precise regulation of the crystalline structure of the material. Lattice doping can alter the electronic structure at atomic level, such as cation ordering, charge redistribution, and the change of metal–oxygen covalency [28, 29]. From a commercial perspective, material cost and electrochemical properties should be the two main considerations. Therefore, cheap and abundant elements (such as Al, Fe, Mg, Ti, Ca, and Mn) might be

preferred for use in layered Ni-rich cathode, while expensive elements (such as Rh, Ru, Ga, and Bi) cannot be used in commercial applications [9, 30]. Due to same valence state, similar ionic radius Al³⁺ to Co³⁺ (0.535 Å vs. 0.545 Å), and the much stronger covalent bond than Co. So, Al doping can reduce the Li⁺/Ni²⁺ mixing to maintain the structural integrity and mitigate the formation of surface residual Li compounds [14, 31]. However, the single modification strategy has little effect on the electrochemical performance at elevated cutoff potential. As far as we know, Ti element can enhance the electronic and ionic conductivity for the charge compensation and the larger ionic radius (0.605 Å) than Co [16, 32]. Consequently, the synergistic effect of Al and Ti cations co-doping strategy may improve the integrity of structure and inhibit the unfavorable phase transformation at different cutoff potential. As far as we know, there are few reports on the co-doping of Al and Ti in LiNi_{0.8}Co_{0.1}Mn_{0.1}O₂ cathode.

Herein, we proposed a novel strategy involving uniform Al and Ti co-doping in LiNi_{0.8}Co_{0.1}Mn_{0.1}O₂ cathode. The modified cathode was obtained by mixing the precursor Ni_{0.8}Co_{0.1}Mn_{0.1}(OH)₂, LiOH·H₂O, Al₂O₃, TiO₂, and subsequent high temperature calcination. The schematic diagram of material preparation is shown in Fig. 1a. Compared with the pristine sample, the modified sample with the incorporation of Al and Ti cations exhibits excellent rate capability and satisfying discharge capacity as well as at elevated cutoff potential.

Experiment section

Materials synthesis

The precursor material was obtained via the traditional hydroxide co-precipitation method. Specifically, the uniformity mixing solution of NiSO₄·6H₂O, CoSO₄·7H₂O, and MnSO₄·5H₂O (in a chemical stoichiometric ratio of Ni/Co/Mn is 8:1:1) was continuously fed into a 500-mL reactor with an appropriate feeding rate. Meanwhile, NH₄OH solution and NaOH solution were fed into the reactor simultaneously at a proper feeding rate and amount. For removing O₂, the atmosphere of the reactor was filled with N₂. The reactor temperature remained at 50 °C, and the pH value of the reactor was maintained accurately at 11.0 via pH meter. After the 12 h

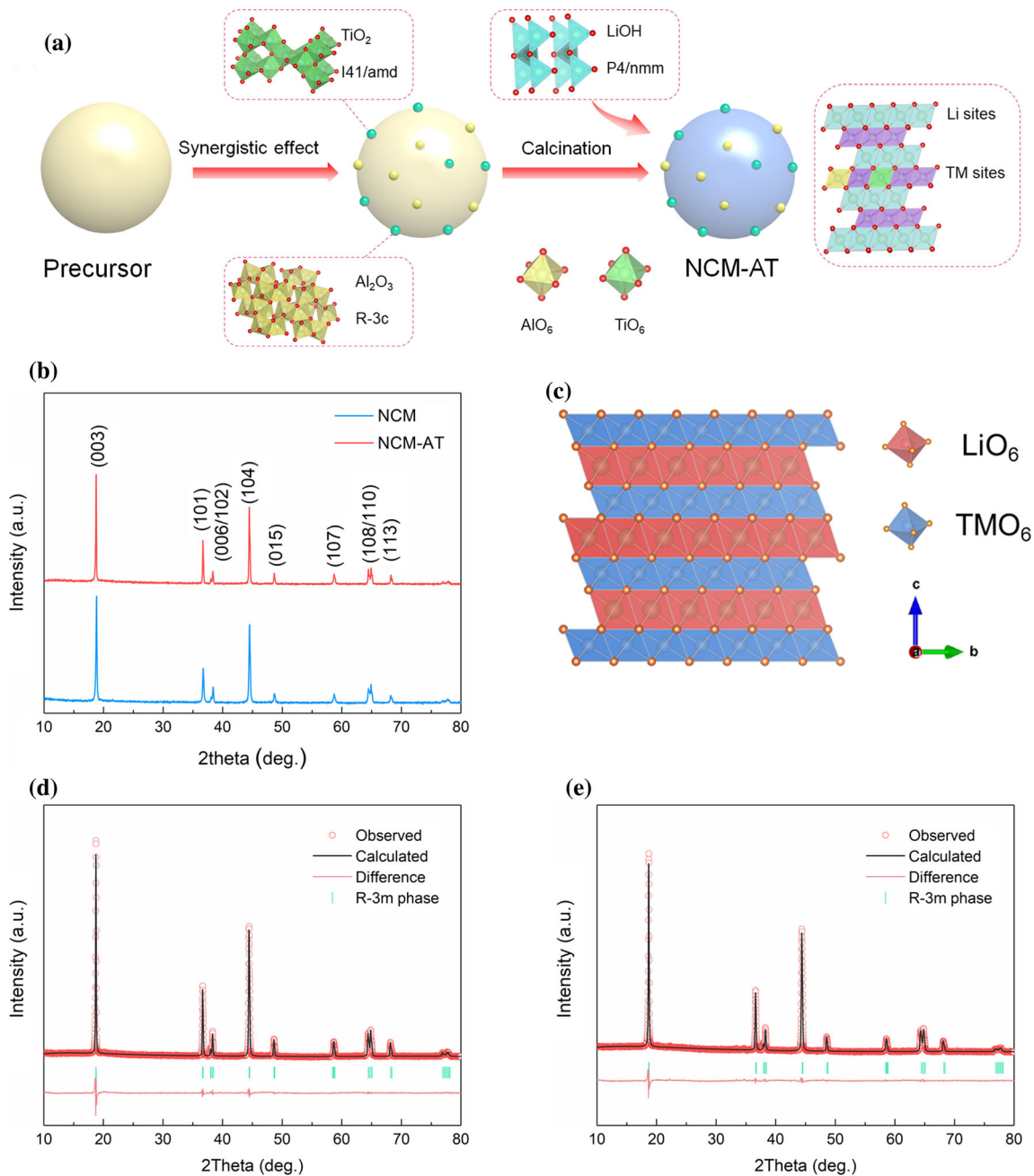


Figure 1 a Schematic illustration of the preparation process. b XRD patterns of NCM and NCM-AT samples. c Crystal structure diagram-based LiMO_2 model. The fitting spectra of Rietveld refinement of NCM (d), and NCM-AT (e).

reaction, the final precipitate was filtered and washed with de-ionized water for several times and dried in a vacuum oven at 120 for 10 h. Finally, the precursor material was mixed with $\text{LiOH}\cdot\text{H}_2\text{O}$ (0.5% excess) for 30 min. The well-mixed material was preheated for 5 h at 480 °C and then heated for 15 h at 820 °C under an oxygen flow, and then naturally cools it to room temperature. The resulting material was labeled NCM. The preparation and calcination

process of the modified material was the same as that of the raw material, only 1 mol % Al_2O_3 and 1 mol % TiO_2 were added in the mixing process and the modified material was labeled NCM-AT.

Materials characterizations

The crystal structure of all samples was detected by powder X-ray diffraction (XRD) using $\text{Cu K}\alpha$

radiation under the angle of 10–80°. The full-pattern refine treatment was obtained via GSAS software. The surface morphology was obtained by scanning electron microscopy (SEM). The surface element distribution was evaluated using energy-dispersive spectroscopy (EDS) mapping. The transmission electron microscope (TEM, FEI) was used to investigate the microstructure or micromorphology. The element's valence state and composition were obtained by the X-ray photoelectron spectroscopy (XPS). The elements binding energies in the spectra of all chemical elements were calibrated by standard C 1 s spectra (284.8 eV), and XPS PeakFit software was performed the spectra fitting of all samples.

Electrochemical measurements

All prepared materials using coin type half-cells (CR2025) to evaluate the electrochemical performance. To obtain the final electrodes, the as-prepared cathode powders, conductive acetylene black, and material binder (weight ratio of 80:13:7) were mixed, and N-methyl pyrrolidone (NMP) is the mixture solvent. After mixing in a ball mill for 20 min at 520 rpm, the mixing slurry was coated on the aluminum foil evenly and dried for 12 h at 120 in a vacuum oven. Then, the coated aluminum foil was punched into a wafer with a diameter of 14 mm, and the loading mass of electrode was approximately 2 mg. Finally, the half-cells were assembled with the Li metal as the counter electrode in a glove box under argon atmosphere. The electrolyte was 1 M LiPF₆ soluble in a mixture of ethylene carbonate (EC) and dimethyl carbonate (DMC) (volume ratio of 1:1). NEWARE software was used for evaluating electrochemical performance. The half-cells were tested in the voltage range of 2.7–4.3 V and 2.7–4.5 V (vs. Li/Li⁺) at room temperature, and 1 C refers to 180 mA g⁻¹. The electrochemical impedance spectroscopy (EIS) was obtained by electrochemical workstation with the frequency (100 kHz – 0.01 Hz).

Results and discussion

Figure 1b shows the XRD patterns of NCM and NCM-AT samples under the angle of 10–80°. All samples exhibit the α -NaFeO₂ layered structure with the space group of R-3 m [33]. Then, the well-ordered layered crystal structure of the two samples can be

indicated by the apparent splitting of (006)/(102) and (108)/(110) pairs. Moreover, there are no other impurity peaks in the two samples, implying that the successful incorporation of Al³⁺ and Ti⁴⁺ into the crystal structure and co-doping has little effect on the layered structure. Based on a layered LiMO₂ model (Fig. 1c), the full-pattern Rietveld refinement was carried out to GSAS software, and the well-fitting spectra are shown in Fig. 1d, e. Typically, the values of R_{wp} and R_p (< 10%) indicate that refinement results are credible (Table 1) [34]. As can be seen the lattice parameters in Table 1, it is easily known that the lattice parameters (i.e., a, c, c/a) of the modified sample are larger slightly than these of the pristine sample. Specifically, the lattice parameters a is 2.872722 and 2.875890 Å, respectively, and the lattice parameters c is 14.204408 and 14.233287 Å, respectively. As is known to all, the parameter of c is related to the lithium ions diffusion channel [35, 36]. Therefore, the larger value of c is beneficial to lithium ions diffusion when repeated cycling process. The increase in lattice parameter c on account of the large radius Ti⁴⁺ (0.605 Å) doping into the bulk structure. Moreover, the c/a value of all materials larger than

Table 1 Refined structure parameters of NCM and NCM-AT

Atom	site	x	y	z	Occupancy	Uiso
NCM ($R_{wp} = 2.11\%$, $R_p = 4.51\%$, $\chi^2 = 4.175$)						
Lattice parameters: a = b = 2.87272(2) Å, c = 14.20440(8) Å						
Li ⁺ /Ni ²⁺ mixing = 2.19% c/a ratio = 4.9445 $I_{(003)}/I_{(104)} = 1.321$						
Li1	3a	0	0	0	0.9781	0.00595
Ni2	3a	0	0	0	0.0219	0.00595
Li2	3b	0	0	0.5	0.0219	0.08782
Ni1	3b	0	0	0.5	0.7781	0.01008
Co	3b	0	0	0.5	0.1000	0.01050
Mn	3b	0	0	0.5	0.1000	0.01050
O	6c	0	0	0.24107	1.0000	0.01003
NCM-AT ($R_{wp} = 2.00\%$, $R_p = 3.52\%$, $\chi^2 = 2.863$)						
Lattice parameters: a = b = 2.87589(0) Å, c = 14.23328(7) Å						
Li ⁺ /Ni ²⁺ mixing = 1.42% c/a ratio = 4.9491 $I_{(003)}/I_{(104)} = 1.384$						
Li1	3a	0	0	0	0.9858	0.01095
Ni2	3a	0	0	0	0.0142	0.01095
Li2	3b	0	0	0.5	0.0142	0.80000
Ni1	3b	0	0	0.5	0.7858	0.01063
Co	3b	0	0	0.5	0.1000	0.01529
Mn	3b	0	0	0.5	0.1000	0.01539
Al	3b	0	0	0.5	0.1000	0.01063
Ti	3b	0	0	0.5	0.1000	0.01063
O	6c	0	0	0.24107	1.0000	0.00952

4.9 also provides further evidence of a well-ordered layered structure. Typically, the Li/Ni mixing deteriorates the electrochemical performance due to the presence of an inactive NiO-like phase. In layered materials (such as NCM811), the ratio of $I_{(003)}/I_{(104)}$ can represent the degree of cations mixing (Li/Ni). And the higher the ratio is, the smaller the mixing degree is [37]. According to the results of Table 1, the value of pristine and modified samples is 1.321 and 1.384, respectively, suggesting that a modified sample possesses low-content Li/Ni mixing. After the refinement of material, the Li/Ni mixing ratio of NCM and NCM-AT is 2.19% and 1.42%, respectively. It can be concluded that the mixing degree of the modified material decreases and the structural stability of the material is improved.

To obtain N-rich with excellent electrochemical performance, it is necessary to design an appropriate precursor for the latter lithiation reaction. The

morphology of precursor is shown in Fig. 2a–c; a spherical secondary particle is composed of primary flake particles via hydroxide co-precipitation method, using to prepare cathode materials. After evenly mixed with lithiation sources and calcined at high temperatures, all obtained materials retain the spherical shape and the secondary particle size was $\sim 10\ \mu\text{m}$ (Fig. 2d–i). The surface morphology of primary particles was different when carefully observed. As can be seen from the yellow ellipse dotted line box from Fig. 2f, i, the secondary particle of NCM-AT is denser, and the porosity of the surface is smaller, implying that Al and Ti co-doping strategy has some effect on the surface morphology where the side reaction between electrolyte and cathode material could be inhibited to some extent. Moreover, to further understand the existence of Al and Ti cations on the NCM-AT material, EDS mapping adopted and the images of the elements of NCM-AT are shown in

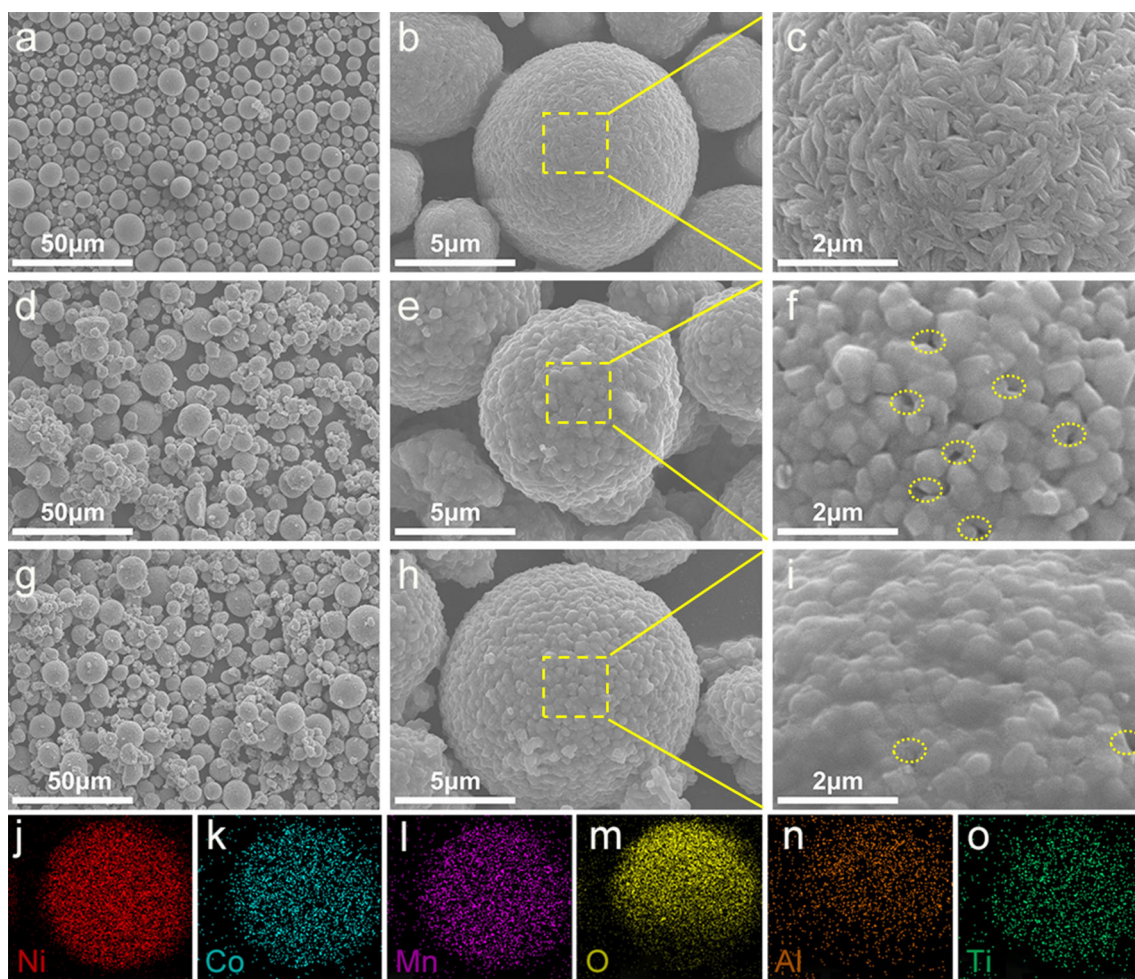


Figure 2 SEM image of precursor (a–c), NCM (d–f) and NCM-AT (g–i). EDS mapping images of NCM-AT sample (j–o).

Fig. 2j–o. It is easy to see the elements of Al and Ti of the NCM-AT surface show a uniform distribution. Therefore, combined with XRD analysis, uniform Al and Ti cations are successfully incorporated into the crystal lattice.

To further investigate the microstructures of materials, HRTEM was performed, and Fig. 3 shows the corresponding images of all materials. Figure 3a and b exhibits the images of primary particles of NCM and NCM-AT, respectively. Taking from the yellow square zone in Fig. 3a, it is easy to see the interplanar spacings of 0.236 nm indicate the well-layered structure of NCM. Moreover, the fast Fourier transformation (FFT) of the white region in the bulk of NCM provides further evidence for the layered structure. Similarly, the (003) crystal plane of the layered structure was detected in the white square zone of NCM-AT material [30, 38]. It can be concluded that the two materials exhibit a high ordered layered phase. In conclusion, this phenomenon reveals that the incorporation of Al and Ti cations is successfully doped into the crystal lattice and is no visible effect on the structure of the material.

To further figure out the valence state's variation of surface elements after modification, XPS analysis was obtained due to its high surface sensitivity. The elements of Ni, Co, Mn, O, Ti, Al, and C were detected in the NCM-AT (Fig. 4a). The binding energy peaks of 73.6 and 457.6 eV are attributed to the Al and Ti 2p (Fig. 4b, c) [39]. It is concluded that Al and Ti cations are successful incorporation into the lattice structure. Normally, the binding energy peaks of Ni^{2+} and Ni^{3+} are approximately 855.20 eV and 856.40 eV, respectively [40]. As shown in Fig. 4d, e, all samples are mixed valence of + 2 and + 3 for Ni oxidation state. Moreover, the ratio of $\text{Ni}^{2+}/\text{Ni}^{3+}$, via the

semiquantitative analysis, for NCM-AT sample, is larger than the NCM sample. As the incorporation of high valence Al^{3+} and Ti^{4+} , for the charge compensation, a fraction of high valence Ni^{3+} reduces to low valence Ni^{2+} . To maintain the structure stability, the Mn oxidation state of all samples remains + 4 in Ni-rich layered materials (Fig. 4f) [41].

The initial charge–discharge curves with the voltage range of 2.7–4.3 V at 0.1 C are shown in Fig. 5a. In the 1st cycle, the specific capacity of pristine and modified samples is 177.32 and 189.70 mAh g^{-1} , and the corresponding coulombic efficiency is 83.79 and 85.45%, respectively. This capacity difference of the two samples may be on account of the enlargement of Li ions diffusion channels and low the cation mixing. Figure 5b shows the cycle life of all materials after 200 charge–discharge cycles at 1 C. The specific capacity retention rate of NCM and NCM-AT is 46.67 and 76.75%, respectively. Remarkably, the material exhibits improved cycle life after the modification. To obtain the excellent cathode of higher energy density LIBs, the constant working voltage is crucial. The average discharge voltage of the two materials during cycling is shown in Fig. 5c. From the 1st cycle to the 200th cycle, the average difference voltage of the NCM sample is 0.377 V, with the voltage retention of 90.04%. In sharp contrast, the average difference voltage of the NCM-AT sample is 0.035 V, with voltage retention of 98.78%. The modified sample exhibits an excellent electrochemical performance of average discharge voltage. Therefore, the co-doping strategy of Al and Ti cations can improve the discharge capacity and inhibit the normal discharge voltage fading during repeated cycling. Figure 5d–f presents different discharge capacity under a different current density of all materials. Comparing with

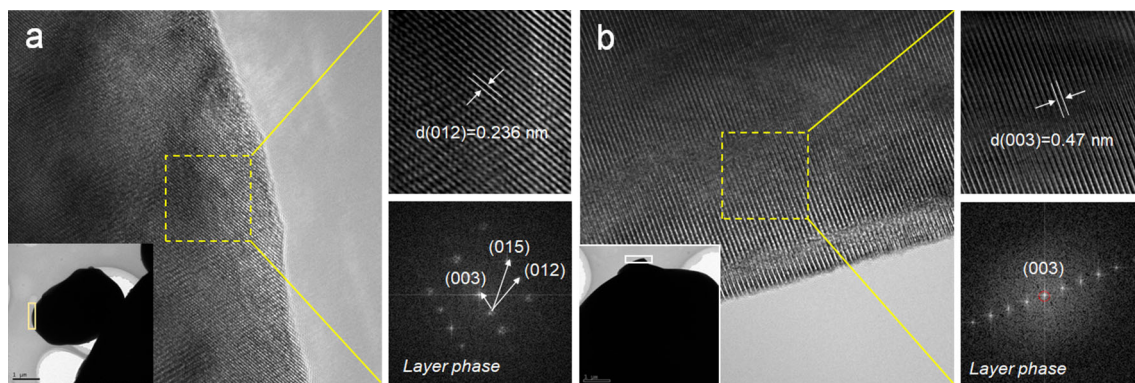


Figure 3 HRTEM image and corresponding FFT pattern of NCM (a) and NCM-AT (b).

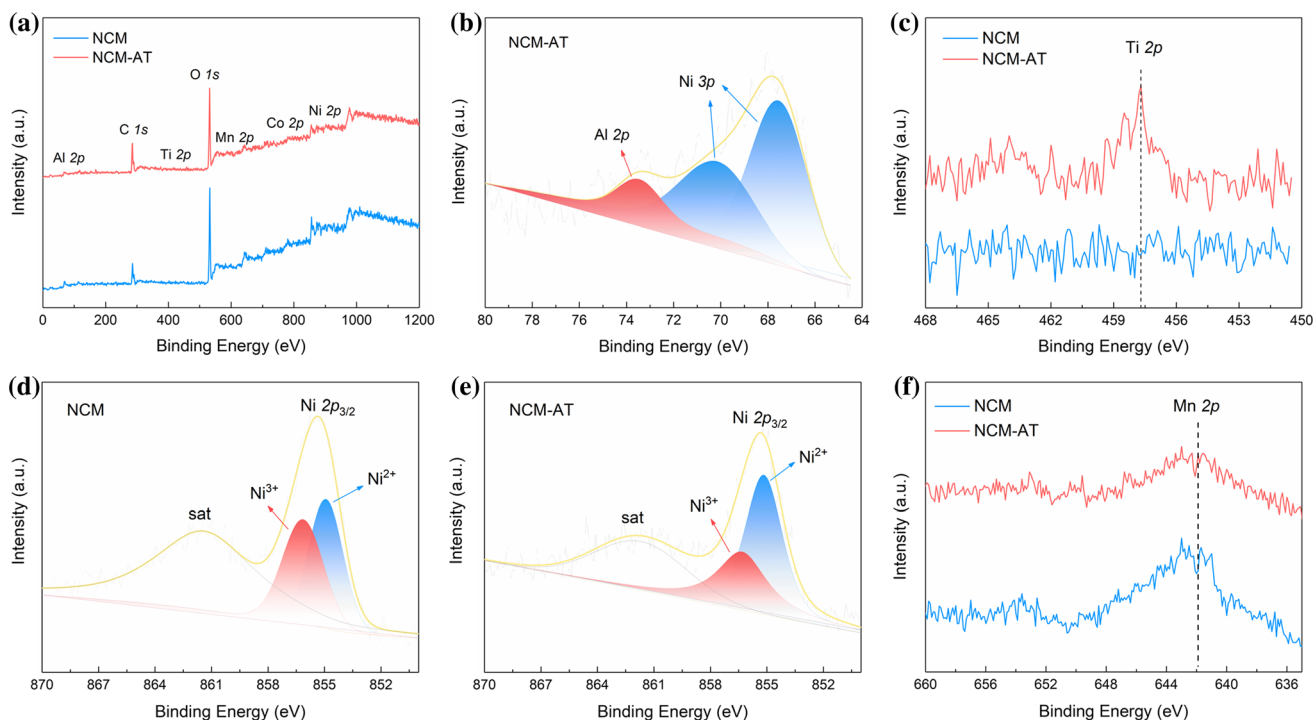


Figure 4 The survey spectrum of all samples (a). XPS spectra of Al 2p (b) for NCM-AT. Ti 2p (c) for all samples. Ni 2p for NCM (d) and NCM-AT (e), and Mn 2p (f) for all samples.

the rate capability of NCM, it is easy to see NCM-AT exhibits the excellent rate capability. Moreover, NCM-AT still possesses a high capacity of 128 mAh g^{-1} at a large current density of 10 C. In comparison, NCM exhibits poor rate capability and attains 105 mAh g^{-1} under the same condition. The improved capability on account of the inactive Al and Ti ions can act as a pillar role when repeatedly cycling, resulting in reduce structure distortion and stabilize the bulk structure. But usually too many foreign ions will hinder the transfer of lithium ions, so it needs to be controlled in a proper number of foreign ions. Moreover, Fig. 5g shows the cycle life of all materials at 10 C. In sharp contrast, after 200 charge/discharge cycles, NCM and NCM-AT exhibit a discharge capacity retention of 29.34 and 73.36%, respectively. Moreover, Fig. 5h depicts the initial charge and discharge curves of all materials between 2.7 and 4.5 V at 0.1 C. During the initial cycle, the discharge capacity of NCM and NCM-AT is 189.25 and $194.21 \text{ mAh g}^{-1}$, and the corresponding coulombic efficiency is 78.08 and 81.62%, respectively. The modified material possesses a high capacity than pristine material. Also, NCM cathode suffers from severe discharge capacity decay. At the 200 cycles, NCM cathode exhibits a capacity of 89.53 mAh g^{-1} with a

capacity retention of 49.44%, while NCM-AT cathode not only increases the capacity but also shows a better cycle life (Fig. 5i). The NCM-AT cathode delivers an improved capacity of $129.24 \text{ mAh g}^{-1}$ with the capacity retention of 70.93%. In summary, the modified materials possess better electrochemical performance at different cutoff voltages.

To explain the enhancement in the electrochemical performance in the discharge capacity retention, the structural changes with electrochemical reactions during cycling were obtained by the dQ/dV profiles at different cutoff voltages (Fig. 6). In general, the multiple peaks represent phase transitions corresponding to the contraction/expansion of lattice parameters. Ni-rich cathode usually underwent several phase transitions, including the hexagonal phase (H1), monoclinic phase (M) at the initial charging stage, and hexagonal phase (H2/H3) at the subsequent charging stage. In this phase transformations, the phase transition of H2/H3 is harmful to the layered phase, causing the bulk structure to collapse and turning the layered phase to the inactive NiO phase [42, 43]. Avoiding the phase transition of H2/H3 is crucial to realize the reversibly of cathodes. The redox peaks for the NCM-AT cathode remain relatively stable and exhibit well reversibly during the

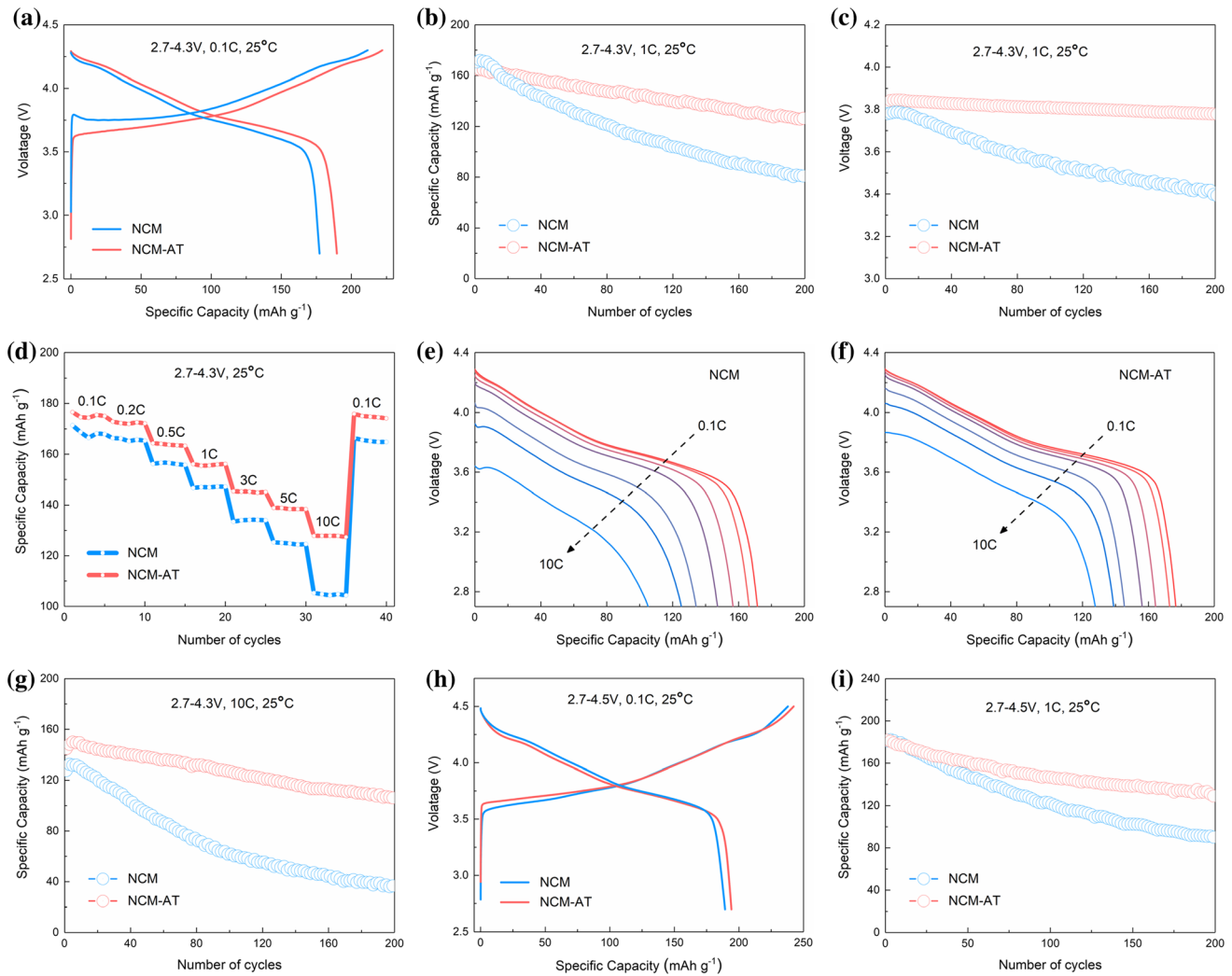


Figure 5 **a** Initial charge–discharge curves between 2.7 and 4.3 V at 0.1 C. **b** Cycle life at 1 C after 200 cycles. **c** Average discharge voltage over the cycling of all materials. **d** Rate performance for

all materials. **e, f** Discharge curves at different current density. **g** Cycle life at 10 C. **h** Initial charge–discharge curves all materials between 2.7 and 4.5 V at 0.1 C. **i** Cycle life at 1 C after 200 cycles.

extend cycles at the voltage range of 2.7–4.3 V (Fig. 6b). In sharp contrast, the NCM cathode shows macroscopic changes and poor reversibility (Fig. 6a). It can be concluded that NCM-AT cathode mitigates the harmful phase transition to achieve superior capacity and voltage retention during cycling. In addition, the dQ/dV profiles at the voltage window of 2.7 and 4.5 V were obtained (Fig. 6c, d). Regarding the NCM cathode, the position of the peak for anodic shifts to higher voltage range and the peaks position for cathodic shifts lower voltage range during 1st to 100th cycling, indicating the severe polarization after repeated delithiation/lithiation process at elevated cutoff voltage. However, the anodic and cathodic peak positions retain relatively stable in NCM-AT

cathode at the same condition. The profile analysis of NCM and NCM-AT shows that the improved samples have good electrochemical reversibility. Because the spinel phase is more stable than the layered structure, the layered phase has irreversible transformation to the thermodynamically stable spinel phase, and the presence of foreign ions inhibits the migration of transition metal ions and is conducive to the maintenance of structural stability and the avoidance of spinel phase transition to some extent [44, 45].

Electrochemical impedance spectroscopy (EIS) was carried to analyze the dynamic behavior. The Nyquist plots of the two cathodes before cycle and after 100 cycles are shown in Fig. 7a. Typically,

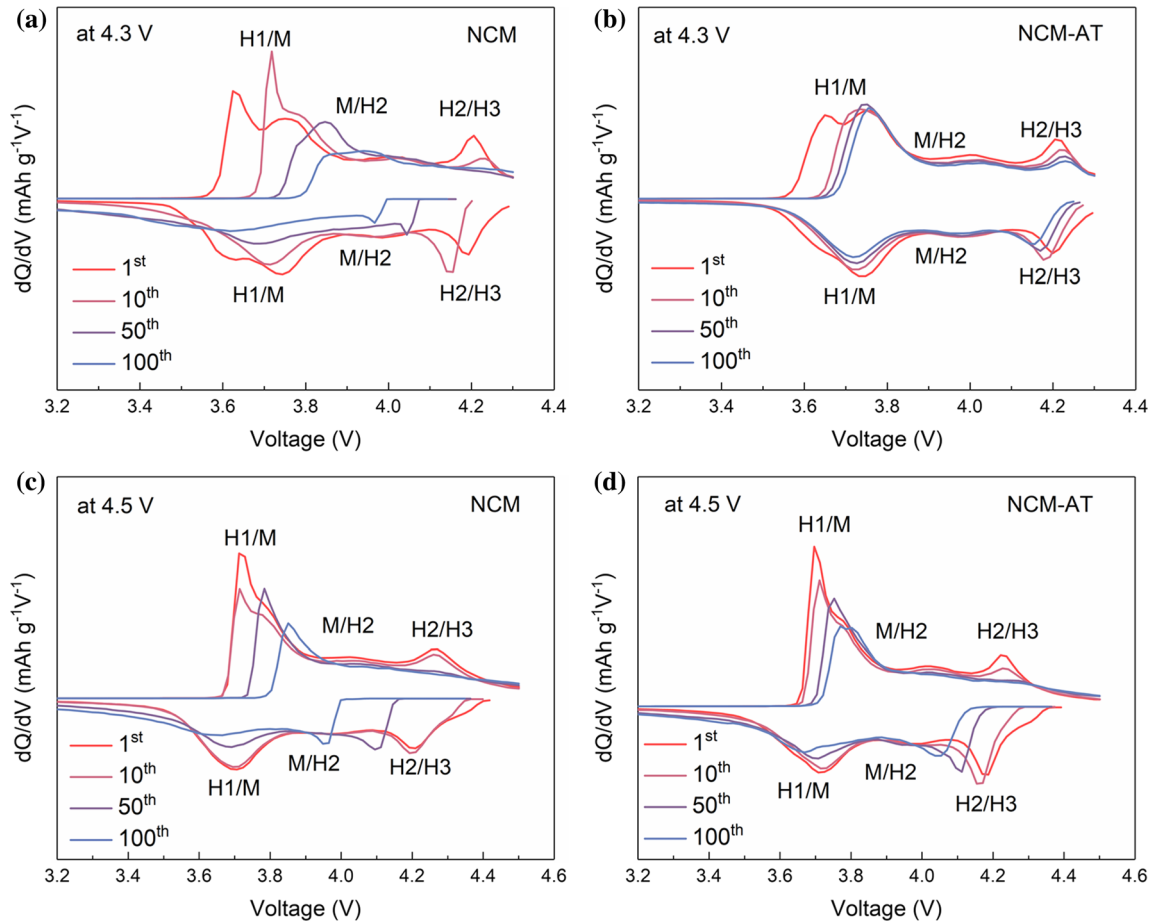


Figure 6 The differential capacity curves of NCM (a) and NCM-AT at different cycles (b) at 2.7–4.3 V, 2.7–4.5 V for NCM (c) and NCM-AT (d).

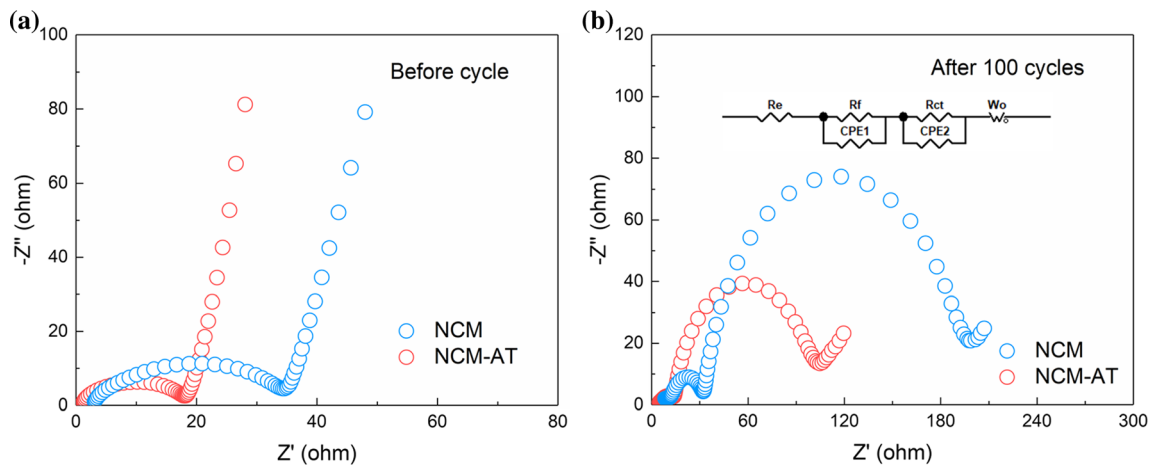


Fig. 7 Nyquist plots of the electrodes (a) before cycle and (b) after 100 cycles of NCM and NCM-AT electrodes.

Nyquist plots are made up of two parts, a semicircle in the medium–high frequency region and a slope line in the low-frequency region [46, 47]. Charge-transfer resistance (Rct) represents charge transfer

impedance, and Warburg impedance (Zw) has a relationship to the diffusion coefficient of lithium ions. The solvent electrolyte resistances are expressed by Re. Moreover, based on the equivalent circuit

model (Fig. 7b inset), the fitting results of R_e , R_f , and R_{ct} showed in Table 2. Before initial cycle, the R_e and R_{ct} values of the NCM sample are 3.06 and 31.53 Ω , respectively. However, the NCM-AT shows the smallest values of R_e and R_{ct} with 1.04 and 17.07 Ω , respectively. As the charge and discharge progresses, after 100 cycles, the values of R_e , R_f , and R_{ct} of NCM are 8.31, 23.67, and 166.76 Ω , respectively. In contrast, the values of R_e , R_f , and R_{ct} of NCM-AT are 4.75, 8.48, and 91.49 Ω . It is evident that the modified material exhibits a low impedance, which may be the result of inhibiting the inactive phase transition. The proper amount of pillar ions introduced can stabilize the structure and maintain the complete lithium ion transport channel. The EIS results analysis also agrees with the dQ/dV profiles. Therefore, the incorporation of Al and Ti into the lattice can reduce the lithium diffusion barrier to promote dynamic behavior during cycling. As is known to all, the lithium ions diffusion coefficient (D_{Li^+}) was evaluated by the EIS pattern and the calculation equations of D_{Li^+} as follows:

$$D_{Li^+} = R^2 T^2 / 2 A^2 n^4 F^4 C^2 \sigma^2 \quad (1)$$

$$Z' = R_f + R_{ct} + \sigma \omega^{-1/2} \quad (2)$$

In the equations, the R refers to the gas constant (8.314 J K⁻¹ mol⁻¹), T represents room temperature (293.15 K), F refers to the Faraday constant (96485 mol⁻¹), A refers to the reaction area of the electrode (1.766×10^{-4} m²), n refers to the number of electrons and losses during cycling, C is the lithium ions concentration, and σ is the Warburg coefficient [47, 48]. According to results from Table 2, the values of diffusion coefficients of NCM sample are 9.17385×10^{-11} , 1.16024×10^{-12} at initial cycle and 100 cycles. In contrast, the NCM-AT sample shows good lithium ion diffusivity under all conditions with 1.02465×10^{-10} and 6.57985×10^{-12} . It can be seen that the modified samples have a high lithium ion

diffusion coefficient, which may be because the mixing degree of Li⁺/Ni²⁺ cations is reduced and the blockage of the diffusion channel is avoided. And this result is consistent with the excellent rate performance of the modified sample.

Conclusion

In summary, we successfully synthesize uniform Al³⁺ and Ti⁴⁺ modified LiNi_{0.8}Co_{0.1}Mn_{0.1}O₂ cathode by a high-temperature solid-phase reaction. The results show that the co-doping strategy can improve the electrochemical performance. XRD and HRTEM results show that the modified material retains the original intact layered structure. The introduction of foreign ions reduces the degree of material mixing, accelerates the lithium ion transfer, and slows down the harmful phase transition to maintain the structural stability. In addition, the electrochemical performance of the material is still good under high voltage. In general, this simple cation co-doping strategy provides a feasible way to develop high energy density lithium ions layered oxide cathode.

Acknowledgements

This work was funded by the project from the National Natural Science Foundation of China (21878195, 21805198), the Distinguished Young Foundation of Sichuan Province (20JCQN0197), and 2019 Strategic cooperation project between Sichuan University and Luzhou Municipal People's Government (No. 2019CDLZ-06).

Compliance with ethical standards

Conflict of interest The authors declare no conflict of interest.

References

- [1] Nayak PK, Erickson EM, Schipper F, Penki TR, Munichandraiah N, Adelhelm P, Sclar H, Amalraj F, Markovsky B, Aurbach D (2018) Review on challenges and recent advances in the electrochemical performance of high capacity Li- and Mn-rich cathode materials for Li-ion batteries. *Adv Energy Mater* 8:1702397

Table 2 The values of R_e , R_f , R_{ct} , and D_{Li^+} for electrodes of all samples

Sample	Cycle	R_e (Ω)	R_f (Ω)	R_{ct} (Ω)	D_{Li^+} (cm ² s ⁻¹)
NCM	1st	3.06		31.53	9.17385×10^{-11}
	100th	8.31	23.67	166.76	1.16024×10^{-12}
NCM-AT	1st	1.04		17.07	1.02465×10^{-10}
	100th	4.75	8.48	91.49	6.57985×10^{-12}

- [2] Wang J, He X, Paillard E, Laszczynski N, Li J, Passerini S (2016) Lithium- and manganese-rich oxide cathode materials for high-energy lithium ion batteries. *Adv Energy Mater* 6:1600906
- [3] Sharifi-Asl S, Lu J, Amine K, Shahbazian-Yassar R (2019) Oxygen release degradation in Li-ion battery cathode materials: mechanisms and mitigating approaches. *Adv Energy Mater* 9:1900551
- [4] Yu H, Zhou H (2013) High-energy cathode materials ($\text{Li}_2\text{MnO}_3\text{--LiMO}_2$) for lithium-ion batteries. *J Phys Chem Lett* 4:1268–1280
- [5] Croy JR, Gutierrez A, He M, Yonemoto BT, Lee E, Thackeray MM (2019) Development of manganese-rich cathodes as alternatives to nickel-rich chemistries. *J Power Sources* 434:226706
- [6] Pei Y, Chen Q, Xiao Y-C, Liu L, Xu C-Y, Zhen L, Henkelman G, Cao G (2017) Understanding the phase transitions in spinel-layered-rock salt system: criterion for the rational design of LLO/spinel nanocomposites. *Nano Energy* 40:566–575
- [7] Zheng J, Myeong S, Cho W, Yan P, Xiao J, Wang C, Cho J, Zhang J-G (2017) Li- and Mn-rich cathode materials: challenges to commercialization. *Adv Energy Mater* 7:1601284
- [8] S. Zhao, K. Yan, J. Zhang, B. Sun, G. Wang (2020) Reviving reaction mechanism of layered lithium-rich cathode materials for high-energy lithium-ion battery. *Angew Chem Int Edn* (2020).
- [9] Wang X, Ding YL, Deng YP, Chen Z (2020) Ni-Rich/Co-poor layered cathode for automotive Li-ion batteries: promises and challenges. *Adv Energy Mater* 10:1903864
- [10] Xu C-L, Xiang W, Wu Z-G, Xu Y-D, Li Y-C, Chen M-Z, Guo X, Lv G-P, Zhang J, Zhong B-H (2018) Constructing a protective pillaring layer by incorporating gradient Mn^{4+} to stabilize the surface/interfacial structure of $\text{LiNi}_{0.815}\text{Co}_{0.15}\text{Al}_{0.035}\text{O}_2$ cathode. *ACS Appl Mater Interfaces* 10:27821–27830.
- [11] Yong-Chun Li WX, Yao Xiao, Zhen-Guo Wu, Chun-Liu Xu, Wei Xu, Ya-Di Xu, Chen Wu, Zu-Guang Yang, Xiao-Dong Guo (2019) Synergy of doping and coating induced heterogeneous structure and concentration gradient in Ni-rich cathode for enhanced electrochemical performance. *J Power Sources* 423:144–151.
- [12] Yong Ming WX, Lang Qiu, Weibo Hua, Rong Li, Zhen-Guo Wu, Chunliu Xu, Yongchun Li, Dong Wang, Yanxiao Chen, Benhe Zhong, Fengrong He, Xiaodong Guo (2019) Dual elements coupling effect induced modification from surface into bulk lattice for Ni-rich cathode with suppressed capacity and voltage decay. *ACS Appl Mater Interfaces* 12:8146–8156.
- [13] Xu C, Xiang W, Wu Z, Xu Y, Li Y, Wang Y, Xiao Y, Guo X, Zhong B (2019) Highly stabilized Ni-Rich cathode material with Mo induced epitaxially grown nanostructured hybrid surface for high-performance Lithium-ion batteries. *ACS Appl Mater Interfaces* 11:16629–16638
- [14] Qiu L, Xiang W, Tian W, Xu C-L, Li Y-C, Wu Z-G, Chen T-R, Jia K, Wang D, He F-R, Guo X-D (2019) Polyanion and cation co-doping stabilized Ni-rich Ni–Co–Al material as cathode with enhanced electrochemical performance for Li-ion battery. *Nano Energy* 63:103818
- [15] Yong-Chun Li WX, Zhen-Guo Wu, Chun-Liu Xu, Ya-Di Xu, Yao Xiao, ZuGuang Yang, Chun-Jin Wu, Gen-Pin Lv, Xiao-Dong Guo (2018) Construction of homogeneously Al^{3+} doped Ni rich Ni-Co-Mn cathode with high stable cycling performance and storage stability via scalable continuous precipitation. *Electrochimica Acta* 291:84–94.
- [16] Feng X, Gao Y, Ben L, Yang Z, Wang Z, Chen L (2016) Enhanced electrochemical performance of Ti-doped $\text{Li}_{1.2}\text{Mn}_{0.54}\text{Co}_{0.13}\text{Ni}_{0.13}\text{O}_2$ for lithium-ion batteries. *J Power Sources* 317:74–80.
- [17] Yang X, Tang Y, Shang G, Wu J, Lai Y, Li J, Qu Y, Zhang Z (2019) Enhanced cyclability and high-rate capability of $\text{LiNi}_{0.88}\text{Co}_{0.095}\text{Mn}_{0.025}\text{O}_2$ cathodes by homogeneous Al^{3+} doping. *ACS Appl Mater Interfaces* 11:32015–32024.
- [18] Wu F, Li Q, L. Chen L, Zhang Q, Wang Z, Lu Y, Bao L, Chen S, Su Y (2019) Improving the structure stability of $\text{LiNi}_{0.8}\text{Co}_{0.1}\text{Mn}_{0.1}\text{O}_2$ by surface perovskite-like $\text{La}_2\text{Ni}_{0.5}\text{Li}_{0.5}\text{O}_4$ self-assembling and subsurface La^{3+} doping. *ACS Appl Mater Interfaces* 11:36751–32024.
- [19] Liu Y, He B, Li Q, Liu H, Qiu L, Liu J, Xiang W, Liu Y, Wang G, Wu Z, Guo X (2020) Relieving capacity decay and voltage fading of $\text{Li}_{1.2}\text{Ni}_{0.13}\text{Co}_{0.13}\text{Mn}_{0.54}\text{O}_2$ by Mg^{2+} and PO_4^{3-} dual doping. *Mater Res Bull* 130:110923.
- [20] Piao JY, Duan SY, Lin XJ, Tao XS, Xu YS, Cao AM, Wan LJ (2018) Surface Zn doped LiMn_2O_4 for an improved high temperature performance. *Chem Commun* 54:5326–5329
- [21] Han B, Xu S, Zhao S, Lin G, Feng Y, Chen L, Ivey DG, Wang P, Wei W (2018) Enhancing the structural stability of Ni-rich layered oxide cathodes with a preformed Zr-concentrated defective nanolayer. *ACS Appl Mater Interfaces* 10:39599–39607
- [22] Liu H, He B, Xiang W, Li YC, Bai C, Liu YP, Zhou W, Chen X, Liu Y, Gao S, Guo X (2020) Synergistic effect of uniform lattice cation/anion doping improved structural and electrochemical performance stability for Li-rich cathode materials. *Nanotechnology* 31:455704
- [23] Mo Y, Guo L, Jin H, Du B, Cao B, Chen Y, Li D, Chen Y (2019) Improved cycling stability of $\text{LiNi}_{0.6}\text{Co}_{0.2}\text{Mn}_{0.2}\text{O}_2$ through microstructure consolidation by TiO_2 coating for Li-ion batteries. *J Power Sources* 448:227439.

- [24] Schipper F, Bouzaglo H, Dixit M, Erickson EM, Weigel T, Talianker M, Grinblat J, Burstein L, Schmidt M, Lampert J, Erk C, Markovsky B, Major DT, Aurbach D (2018) From surface ZrO_2 coating to bulk Zr doping by high temperature annealing of Nickel-rich lithiated oxides and their enhanced electrochemical performance in lithium ion batteries. *Adv Energy Mater* 8:1701682
- [25] Chong S, Chen Y, Yan W, Guo S, Tan Q, Wu Y, Jiang T, Liu Y (2016) Suppressing capacity fading and voltage decay of Li-rich layered cathode material by a surface nano-protective layer of CoF_2 for lithium-ion batteries. *J Power Sources* 332:230–239
- [26] Chen C, Geng T, Du C, Zuo P, Cheng X, Ma Y, Yin G (2016) Oxygen vacancies in SnO_2 surface coating to enhance the activation of layered Li-Rich $Li_{1.2}Mn_{0.54}Ni_{0.13}Co_{0.13}O_2$ cathode material for Li-ion batteries. *J Power Sources* 331:91–99.
- [27] Liu Y, Lin X-J, Sun Y-G, Xu Y-S, Chang B-B, Liu C-T, Cao A-M, Wan L-J (2019) Precise surface engineering of cathode materials for improved stability of Lithium-ion batteries. *Small* 15:1901019
- [28] Sun H-H, Ryu H-H, Kim U-H, Weeks JA, Heller A, Sun Y-K, Mullins CB (2020) Beyond doping and coating: prospective strategies for stable high-capacity layered Ni-rich cathodes. *ACS Energy Lett* 5:1136–1146
- [29] Wen Liu PO, Xien Liu, Min-Joon Lee, Woongrae Cho, Sujong Chae, Youngsik Kim, Jaephil Cho (2014) Nickel-rich layered lithium transition-metal oxide for high-energy lithium-ion batteries. *Angew Chem-Int Edition* 54:4440–4457.
- [30] Manthiram A (2020) A reflection on lithium-ion battery cathode chemistry. *Nat Commun* 11:1550
- [31] Liang Y, Li S, Xie J, Yang L, Li W, Li C, Ai L, Fu X, Cui X, Shangguan X (2019) Synthesis and electrochemical characterization of Mg-Al co-doped Li-rich Mn-based cathode materials. *New J Chem* 43:12004–12012
- [32] Zhang J-N, Li Q, Ouyang C, Yu X, Ge M, Huang X, Hu E, Ma C, Li S, Xiao R, Yang W, Chu Y, Liu Y, Yu H, Yang X-Q, Huang X, Chen L, Li H (2019) Trace doping of multiple elements enables stable battery cycling of $LiCoO_2$ at 4.6 V. *Nat Energy* 4 :594–603.
- [33] Weibo Hua MC, Björn Schwarz, Michael Knapp, Michael Bruns, Juri Barthel, Xiushan Yang, Florian Sigel, Raheleh Azmi, Anatoliy Senyshyn, Alkesandr Missiul, Laura Simonelli, Martin Etter, Suning Wang, Xiaoke Mu, Andy Fiedler, Joachim R. Binder, Xiaodong Guo, Shulei Chou, Benhe Zhong, Sylvio Indris, Helmut Ehrenberg (2019) Lithium/oxygen incorporation and microstructural evolution during synthesis of Li-rich layered $Li[Li_{0.2}Ni_{0.2}Mn_{0.6}]O_2$ Oxides. *Adv Energy Mater* 9:1803094.
- [34] Wen Yang WX, Yanxiao Chen, Zhen-Guo Wu, Weibo Hua, Lang Qiu, Fengrong He, Jun Zhang, Benhe Zhong, Xiaodong Guo (2019) Interfacial regulation of Ni-rich cathode materials with ion conductive and pillaring layer by infusing gradient boron for improved cycle stability. *ACS Appl Mater Interfaces* 12:10240–10251.
- [35] Lee DK, Park SH, Amine K, Bang HJ, Parakash J, Sun YK (2006) High capacity $LiLi_{0.2}Ni_{0.2}Mn_{0.6}O_2$ cathode materials via a carbonate co-precipitation method. *J Power Sources* 162:1346–1350.
- [36] Shi J-L, Xiao D-D, Ge M, Yu X, Chu Y, Huang X, Zhang X-D, Yin Y-X, Yang X-Q, Guo Y-G, Gu L, Wan L-J (2018) High-capacity cathode material with high voltage for Li-ion batteries. *Adv Mater* 30:1705575
- [37] Zhang S, Ma J, Hu Z, Cui G, Chen L (2019) Identifying and addressing critical challenges of high-voltage layered ternary oxide cathode materials. *Chem Mater* 31:6033–6065
- [38] Kalluri S, Yoon M, Jo M, Park S, Myeong S, Kim J, Dou SX, Guo Z, Cho J (2017) Surface engineering strategies of layered $LiCoO_2$ cathode material to realize high-energy and high-voltage Li-ion cells. *Adv Energy Mater* 7:1601507
- [39] Wang L, Ma J, Wang C, Yu X, Liu R, Jiang F, Sun X, Du A, Zhou X, Cui G (2019) A novel bifunctional self-stabilized strategy enabling 4.6 V $LiCoO_2$ with excellent long-term cyclability and high-rate capability. *Adv Sci* 6:1900355.
- [40] Ya-Di Xu JZ, Zhen-Guo Wu, Chun-Liu Xu, Yong-Chun Li, Wei Xiang, Yuan Wang, Yan-Jun Zhong, Xiao-Dong Guo, Hong Chen (2019) Stabilizing the structure of Nickel-rich lithiated oxides via Cr doping as cathode with boosted high-voltage/temperature cycling performance for Li-ion battery. *Energy Technol* 8:1900498.
- [41] Li R, Ming Y, Xiang W, Xu C, Feng G, Li Y, Chen Y, Wu Z, Zhong B, Guo X (2019) Structure and electrochemical performance modulation of a $LiNi_{0.8}Co_{0.1}Mn_{0.1}O_2$ cathode material by anion and cation co-doping for lithium ion batteries. *RSC Adv* 9:36849–36857.
- [42] Hoon-Hee Ryu K-JP, Dae Ro Yoon, Assylzat Aishova, Chong S. Yoon, Yang-Kook Sun (2019) $Li[Ni_{0.9}Co_{0.09}W_{0.01}]O_2$: a new type of layered oxide cathode with high cycling stability. *Adv Energy Mater* 9:1902698.
- [43] Yang H, Wu H-H, Ge M, Li L, Yuan Y, Yao Q, Chen J, Xia L, Zheng J, Chen Z, Duan J, Kisslinger K, Zeng XC, Lee W-K, Zhang Q, Lu J (2019) Simultaneously dual modification of Ni-rich layered oxide cathode for high-energy lithium-ion batteries. *Adv Func Mater* 29:1808825
- [44] Cho Y, Lee S, Lee Y, Hong T, Cho J (2011) Spinel-layered core-shell cathode materials for Li-ion batteries. *Adv Energy Mater* 1:821–828
- [45] Pei Y, Xu C-Y, Xiao Y-C, Chen Q, Huang B, Li B, Li S, Zhen L, Cao G (2017) Phase transition induced synthesis of

- layered/spinel heterostructure with enhanced electrochemical properties. *Adv Func Mater* 27:1604349
- [46] Guowen Song HZ, Zhen Wang, Yanyang Dai, Xiang-yang Zhou, and Juan Yang (2019) Interfacial film $\text{Li}_{1.3}\text{Al}_{0.3}\text{Ti}_{1.7}\text{PO}_4$ coated $\text{LiNi}_{0.6}\text{Co}_{0.2}\text{Mn}_{0.2}\text{O}_2$ for long cycle stability of lithium-ion batteries. *ACS Appl Energy Mater* 2:7923–7932.
- [47] Cao Y, Qi X, Hu K, Wang Y, Gan Z, Li Y, Hu G, Peng Z, Du K (2018) Conductive polymers encapsulation to enhance electrochemical performance of Ni-Rich cathode materials for Li-ion batteries. *ACS Appl Mater Interfaces* 10:18270–18280
- [48] Ran Q, Zhao H, Shu X, Hu Y, Hao S, Shen Q, Liu W, Liu J, Zhang M, Li H, Liu X (2019) Enhancing the electrochemical performance of Ni-rich layered oxide cathodes by combination of the gradient doping and dual-conductive layers coating. *ACS Appl Energy Mater* 2:3120–3130

Publisher's Note Springer Nature remains neutral with regard to jurisdictional claims in published maps and institutional affiliations.